Supporting Information

Templated Self-assembly of a PS-*branch*-PDMS Bottle Brush Copolymer

Li-Chen Cheng[1], Karim R. Gadelrab[1], Ken Kawamoto[2], Kevin G. Yager[3], Jeremiah A. Johnson[2], Alfredo Alexander-Katz[1], and Caroline A. Ross[1]

[1]Department of Materials Science and Engineering and [2]Department of Chemistry, Massachusetts Institute of Technology, Cambridge, MA, 02139, USA

[3]Center for Functional Nanomaterials, Brookhaven National Laboratory, Upton, NY, 11973, USA.

Table S1. Principal q and d for branched macromonomers (MM) and bottle brush copolymer with different degree of polymerization (DP)

Sample Composition	Backbone DP	Principal q (nm^{-1})	d (nm)
PS-15.3k-*branch*-PDMS-5k	MM	0.324	19.4
	10	0.292	21.5
	30	0.287	21.9
	40	0.287	21.9

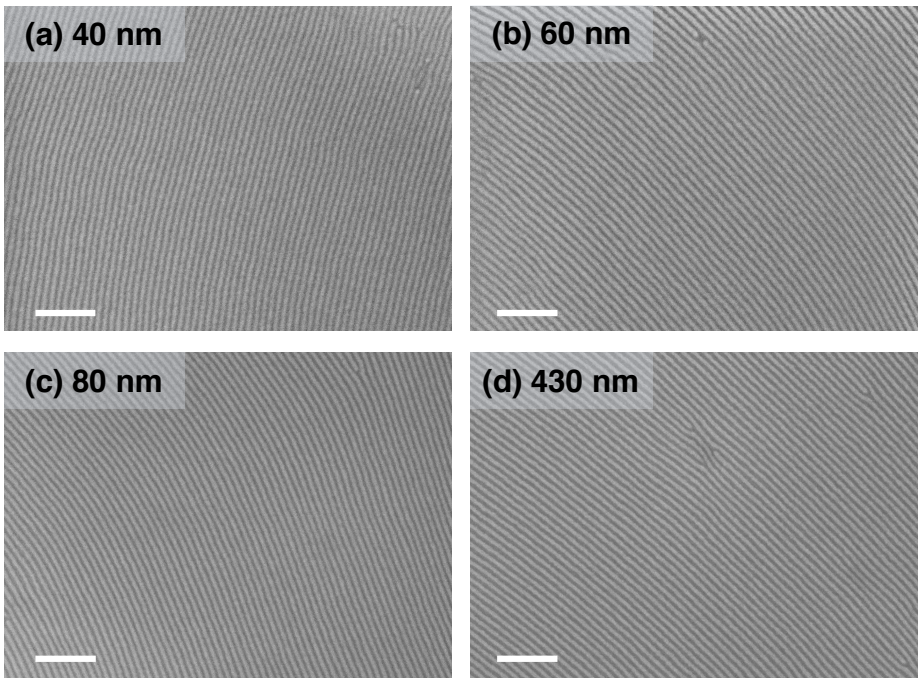

Figure S1. The self-assembled morphologies of $(PS_{15.3k}$-*branch*-$PDMS_{5k})_{30}$ films with various initial film thickness. Top-view SEM images of the self-assembled morphology after solvent annealing under pure toluene vapor at a swelling ratio of 2.5 for 30 min. (a) 40 nm as-cast thickness; (b) 60 nm; (c) 80 nm; (d) 430 nm. Scale bars = 200 nm.

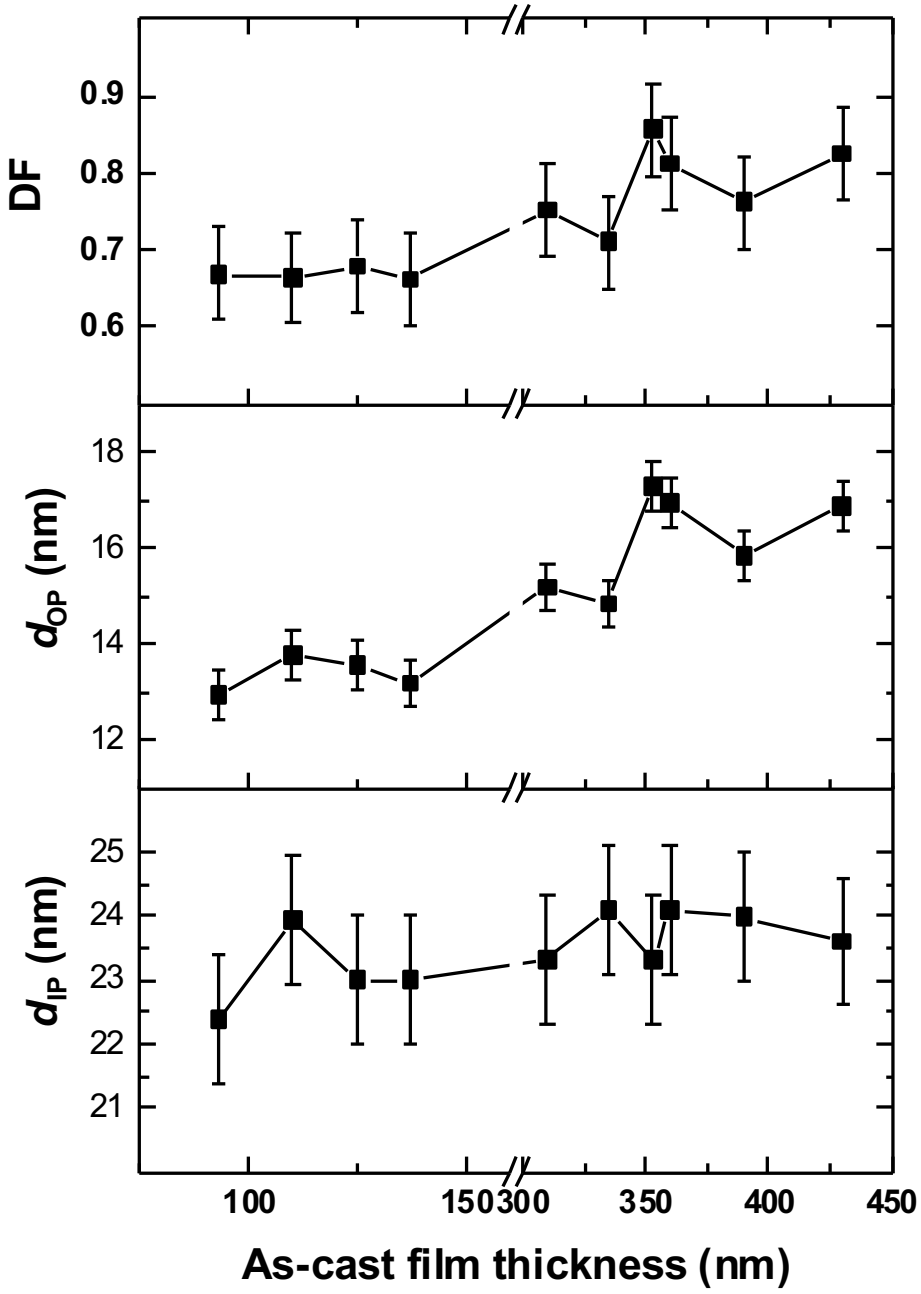

Figure S2. Plots of distortion factor (DF), periodicity of in-plane (IP) and out-of-plane (OP) oriented cylinders in BBCP films with various as-cast film thickness after deswelling. The sample were annealed under pure toluene solvent vapor at swelling ratio of 2.5 for 30 min and deswelled by a flow of 10 sccm N_2 gas for 5 min.

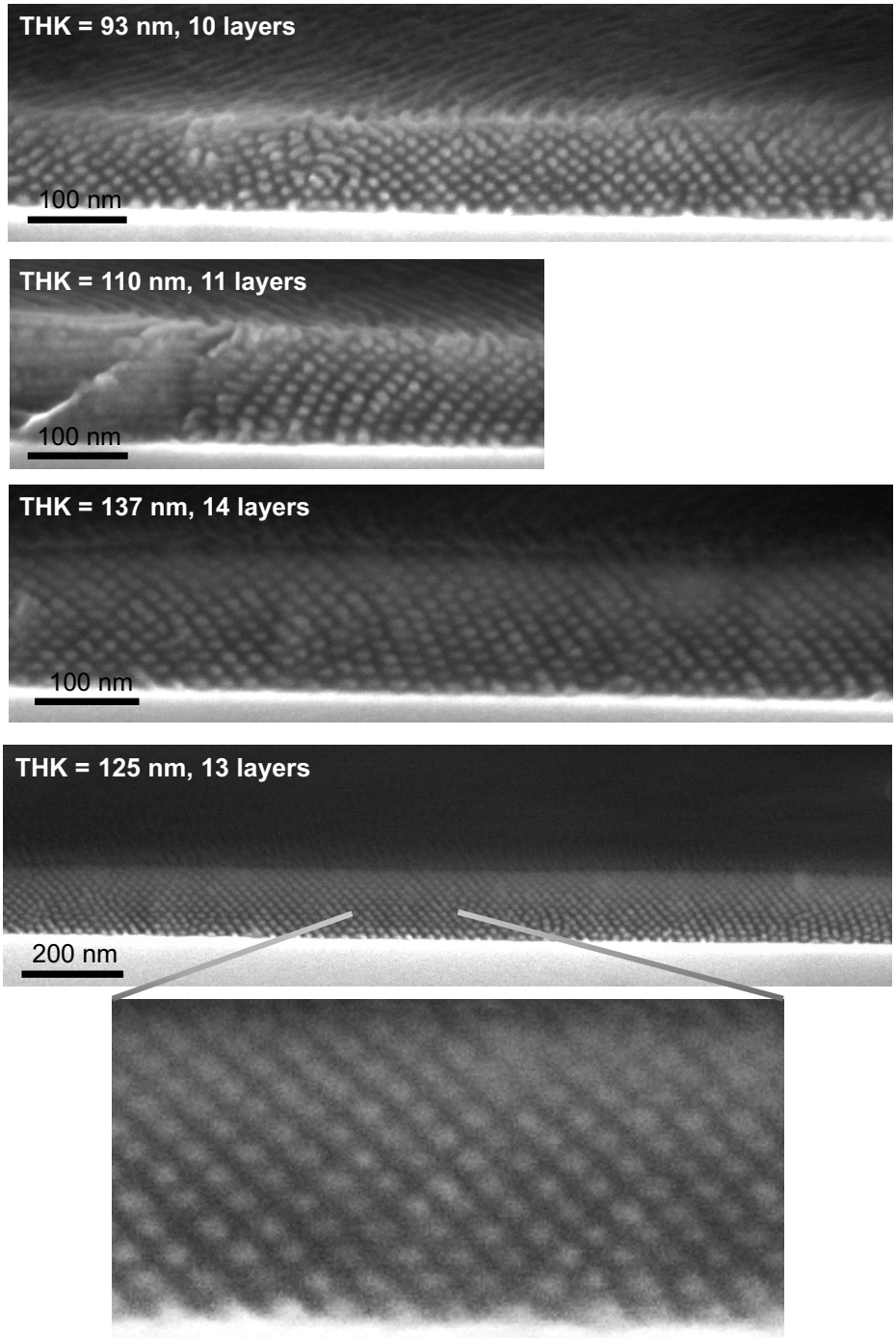

Figure S3. SEM cross-section images of arrays of in-plane cylinder obtained from samples with different as-cast film thickness.

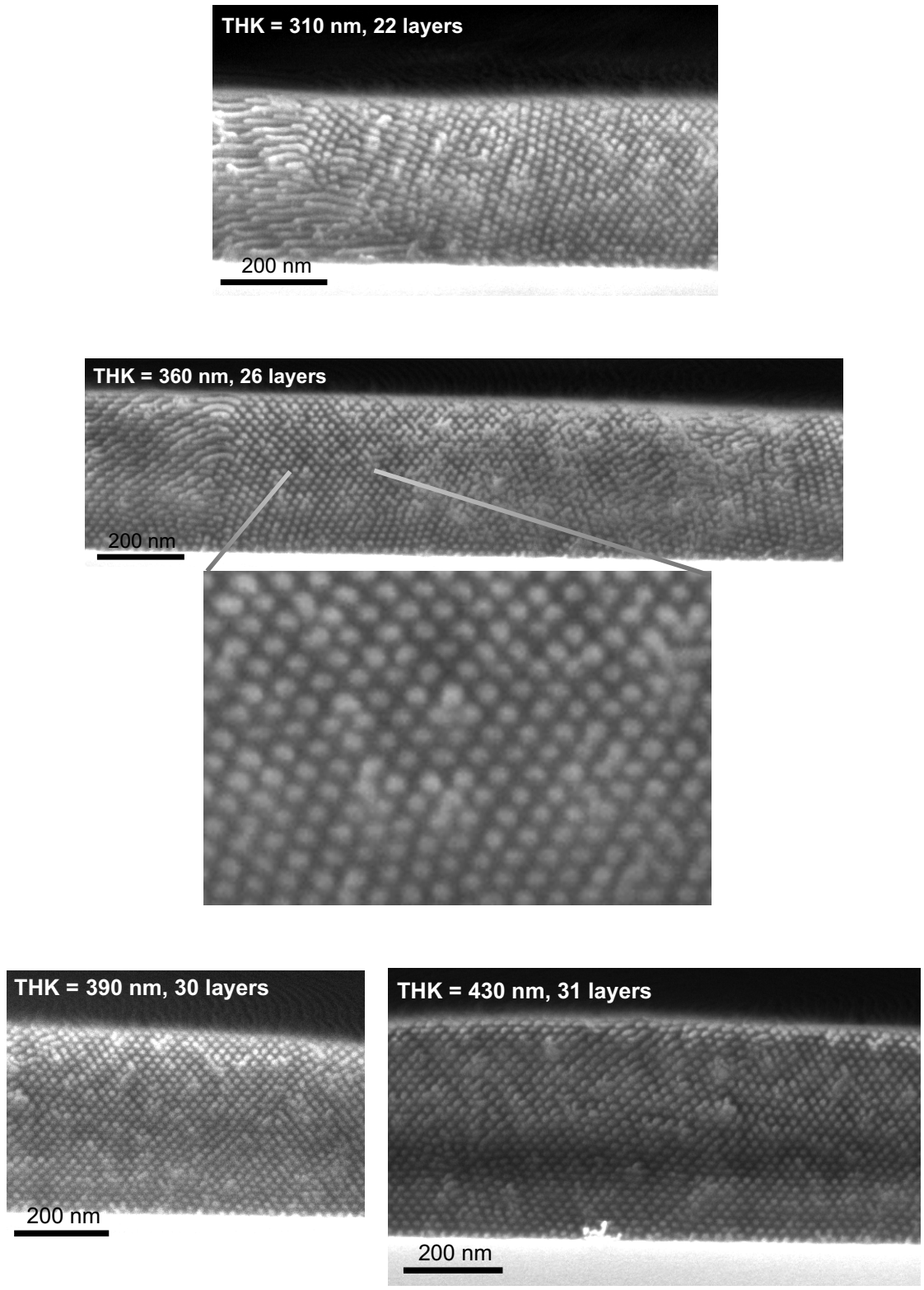

Figure S3. Continued.

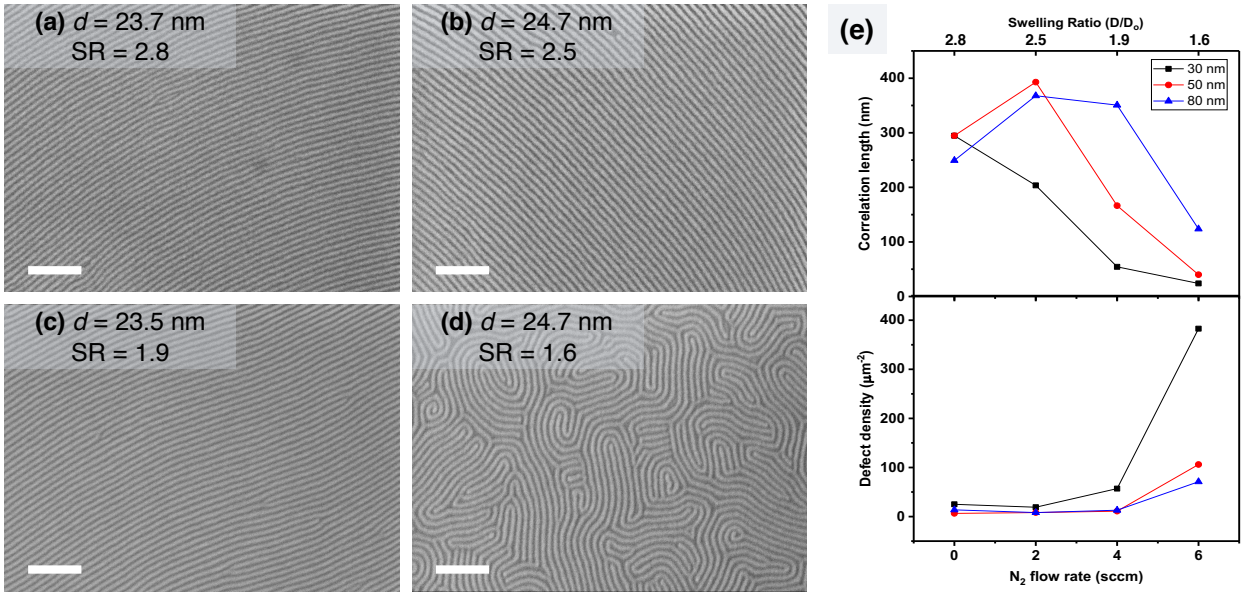

Figure S4. The effect of solvent vapor pressure on the self-assembled morphology of ($PS_{15.3k}$-*branch*-$PDMS_{5k})_{30}$. Top-down SEM images were obtained from samples with as-spun thickness of 50 nm, solvent annealed under pure toluene vapor at a swelling ratio (SR) of (a) 2.8, (b) 2.5, (c) 1.9, (d) 1.6 for 30 min. The self-assembled repeat-spacing *d* are labeled on the images. Scale bars = 200 nm. (e) Plots of microdomain correlation length and defect density as a function of swelling ratio for different as-cast film thicknesses. The swelling ratio was controlled by the vapor flow rate of nitrogen gas from 0 to 6 sccm.

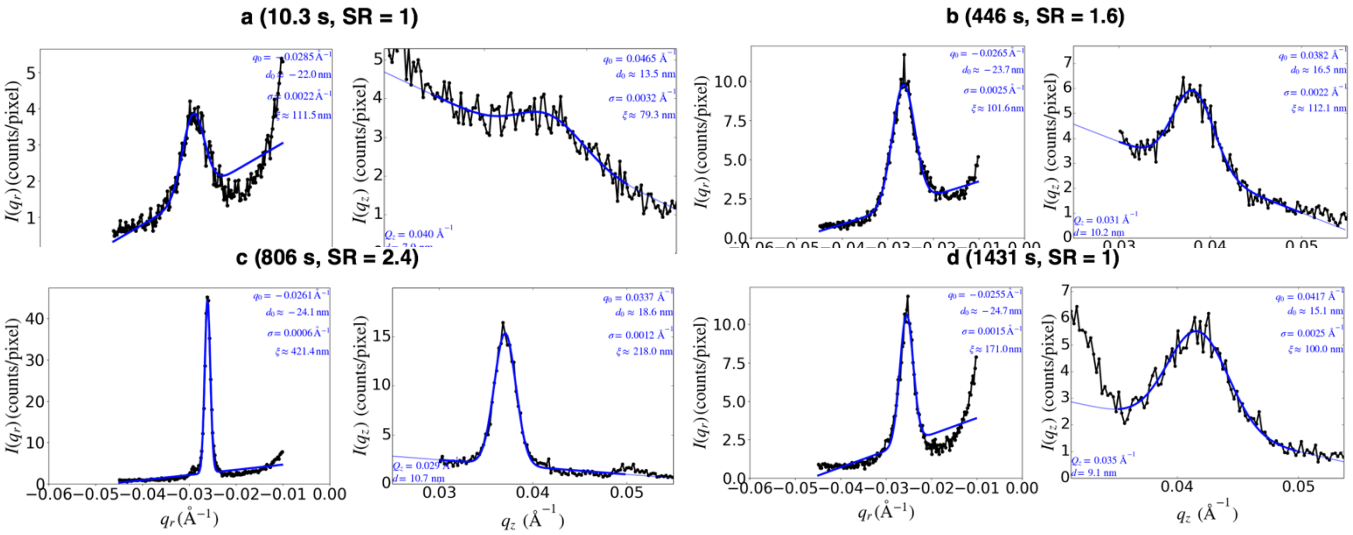

Figure S5. The intensity profiles from the GISAXS patterns in Figure 3c which were measured at different times throughout the solvent anneal. The position of a first-peak along horizontal direction is denoted as $q_r\,(\text{Å}^{-1})$, a first-peak along vertical direction is denoted as $q_z\,(\text{Å}^{-1})$, the real space periodicity is denoted as d_0, the full width at half maximum (FWHM) is denoted as $\sigma(\text{Å}^{-1})$, and the grain-size correlation length is denoted as ξ(nm).

q_z value conversion:

Peaks in GISAXS data were fit to a simple model of a Gaussian with a linear baseline. The center of the Gaussian peak was used to extract a nominal q_z value; that is, the q_z peak position in the detector space. This value must be shifted to account for the refraction effects inherent to GISAXS geometry. In particular, an x-ray beam incident upon a film (at angle θ_i) is refracted upon entering the thin film, and the scattering is refracted as it exits the film. The extent of the refraction depends upon these angles, and the refractive index (for x-rays) of the film. For the materials studied herein, we compute a critical angle of θ_c = 0.09º at an x-ray energy of 13.5 keV (which is confirmed by measuring the position of the Yoneda streak on the detector image). We convert from detector q_z into scattering angle ($2\theta_s$) using $k = 2\pi/\lambda$, where λ is the x-ray wavelength:

$$2\theta_s = 2\sin^{-1}\left[\frac{q_z}{2k}\right]$$

The exit angle of the scattering (above the film horizon) is then $\theta_f = 2\theta_s - \theta_i$. The amount of refraction distortion is calculated through appropriate application of Snell's law:

$$\Delta q_z = q_z - 2k \sin\left(\frac{1}{2}\cos^{-1}\left[\frac{\cos\theta_f}{\cos\theta_c}\right] + \frac{1}{2}\cos^{-1}\left[\frac{\cos\theta_i}{\cos\theta_c}\right]\right)$$

The true reciprocal-space peak position is then obtained by removing the refraction shift: $Q_z = q_z - \Delta q_z$. For the analysis of an in-plane aligned hexagonal lattice of cylinders (i.e. cylinder long-axes in the plane of the film), we cannot directly measure the peak at $q_r = 0$, owing to the intensity of the specular rod and the blocking of the beamstop. Instead, we measure a peak located at 60º with respect to the vertical. The Q_z positions of these peaks are related by a factor of 2. Thus the layering of cylinder rows can be computed using:

$$d = \frac{2\pi}{2Q_z}$$

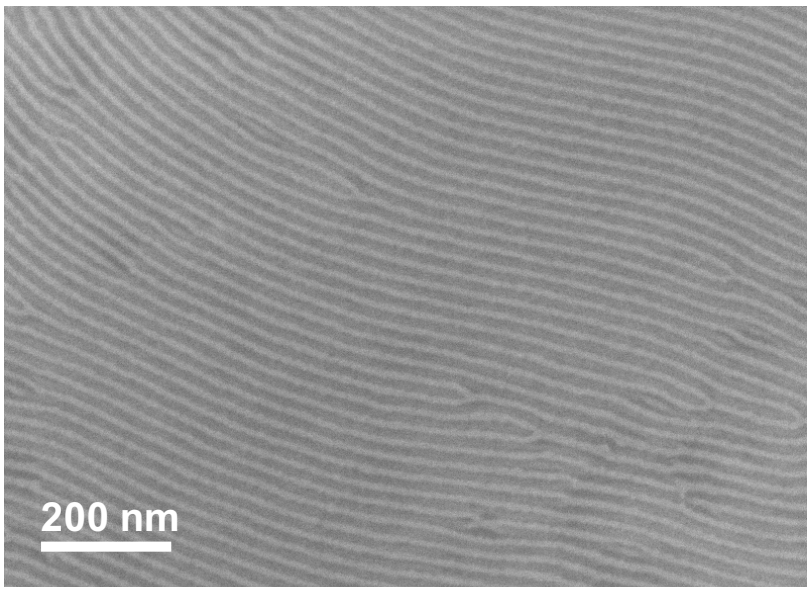

Figure S6. Top-view of SEM images of the self-assembled morphology after etching of 109 nm thick thin films of $(PS_{15.3K}\text{-branch-}PDMS_{5k})_{30}$ after solvent annealing under pure toluene vapor at a swelling ratio of 2.4.

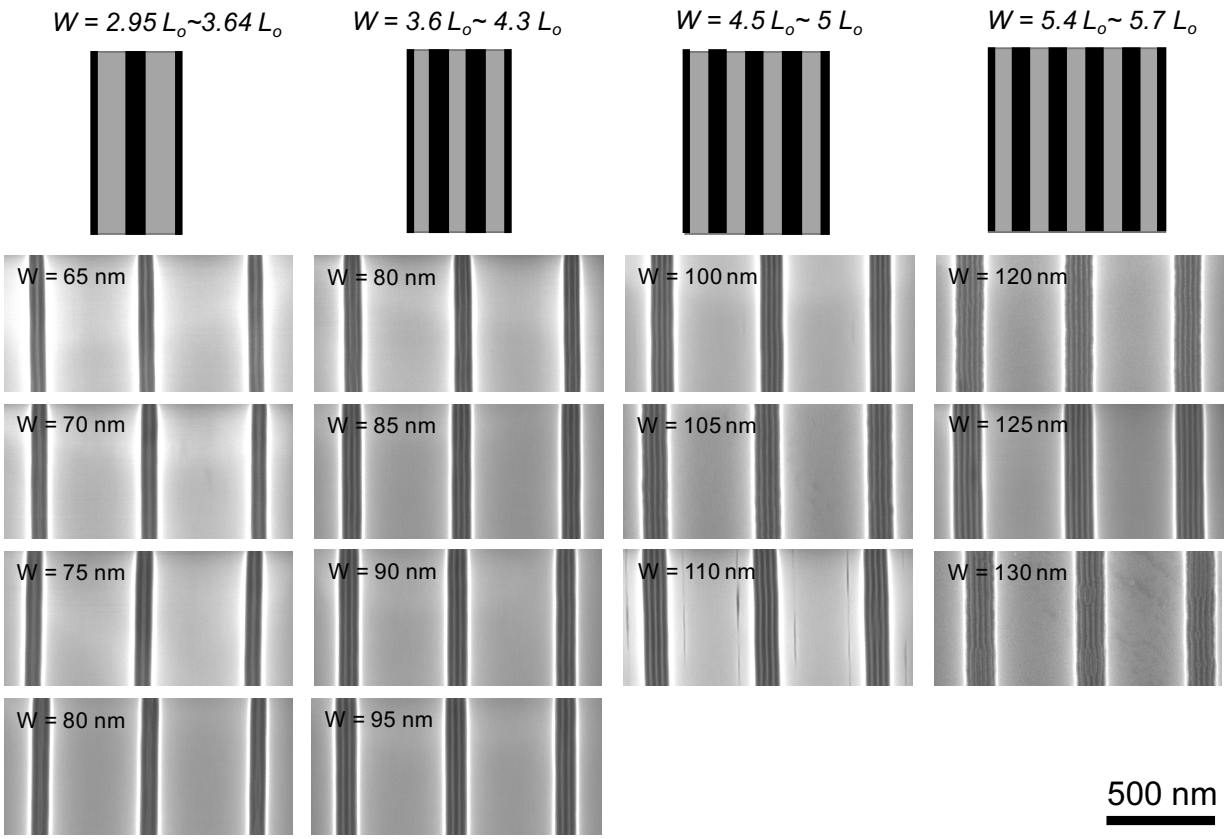

Figure S7. Templated self-assembly of BBCP in the narrow topographic confinements ($2L_0 \leq$ W $\leq 8L_0$). Top-view SEM images of ordered arrays of oxidized PDMS microdomains within gratings of different groove widths W, with number of cylinder rows in the groove *M* varied from 1 to 7 rows. As PDMS block preferentially wets the silica substrate, a thin PDMS wetting layer near trench side wall is expected, as seen in the schematic plots. However, in the SEM images, the thin wetting layer of PDMS cannot be distinguished from the edge of the silica trench after being transformed into silica-like structure by O_2 plasma. Noted that the wetting layer of PDMS was not taken into account for the calculated trench width.

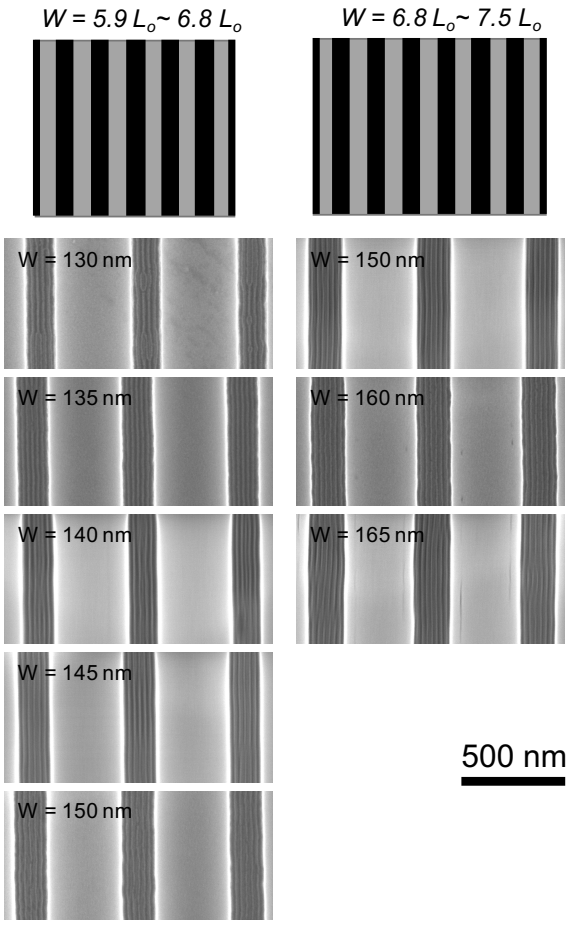

Figure S7. Continued.

Template Fabrication Process:

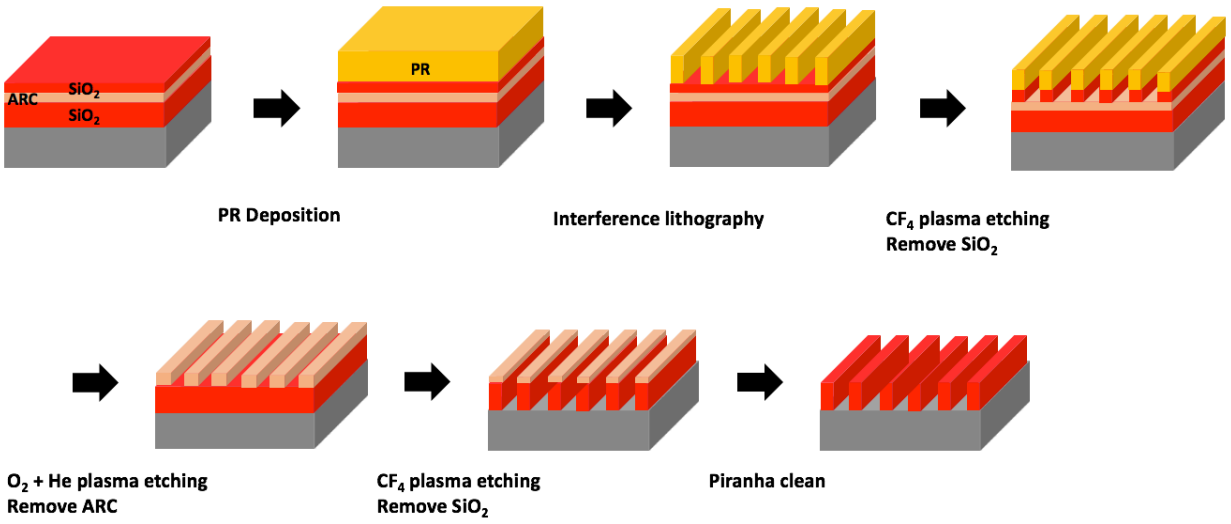

Figure S8. Schematic of fabrication of topographic templates

First, an underlying film stack was formed by depositing a 100 nm silicon oxide film on the Si wafer via electron beam evaporation, spin-coating a layer of inorganic antireflective coating (ARC), and subsequently evaporating a 20 nm silicon oxide film. Next, the grating patterns were fabricated using a Lloyd's Mirror interference lithography system, in which a 325 nm wavelength He-Cd coherent light beam exposed periodic grating patterns into a 200 nm thick positive PFI-88 photoresist (PR). The resultant groove width and grating pitch are determined by the beam exposure time (240 – 300 s). The developed photoresist patterns (MF CD-26 developer) were trim-etched and transferred into the underlying SiO_2 and ARC layer by CF4 plasma for 45 s and a mixture of O_2 plasma and He for 180 s, respectively. A 3 min CF4 plasma etching was used to transfer the grating pattern into the 100 nm SiO_2 layer which serves as the topographical confinement. Finally, a piranha etch was conducted to remove the residual ARC layer and to clean the templates.

Theoretical Model

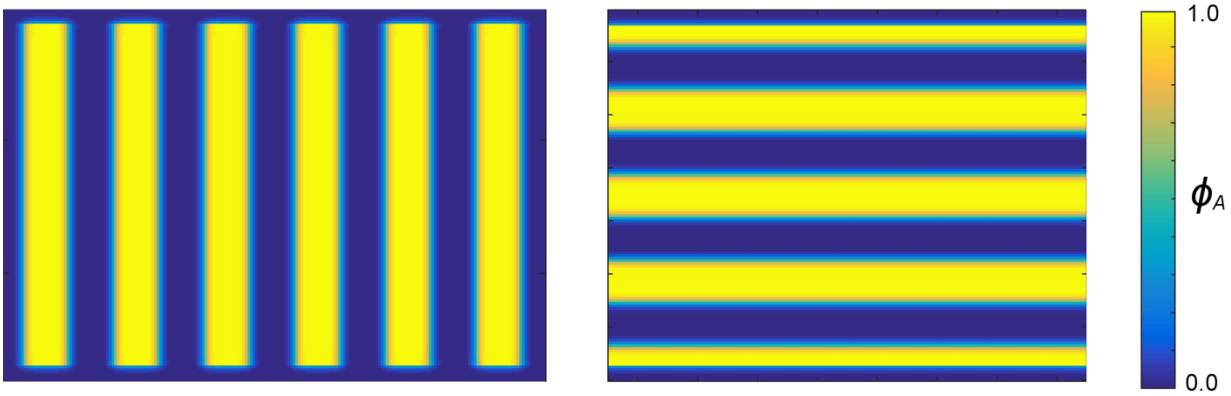

Figure S9. SCFT Density profile of block A in 2D for an m = 29 BBCP. The density shows a striped structure perpendicular and parallel to confining walls (top and bottom of computational cell) used to analyze ΔF at different wall separation.

We study the effect of the polymer architecture of an $(AB)_mC_{m+1}$ block polymer on the characteristics of its self-assembly. The system consists of n bottlebrush molecules with degree of polymerization N_t in a volume V, where every molecule has m AB sidechains dividing the C backbone into m+1 equal segments. N_A and N_B refer to the degree of polymerization of the sidechains A and B, respectively. N_C is the degree of polymerization of the backbone segment between branching points. Hence, $N_t = m(N_A+N_B)+(m+1)N_C$. For simplicity, all molecules are assumed to have equal statistical segment length b and the melt is incompressible. The total block volume fractions are calculated as follows $f_j = mN_j/N_t$ for $j = A$ and B and $f_C = (m+1)N_C/N_t$. The AB degree of polymerization N is kept fixed, where $N = N_A+N_B = 100$. As a result, N_t is a variable that depends on both N_C and m that sets $\alpha = N_t/N$. For all spatial dimensions, we employ a reference radius of gyration $R_g = b(N/6)^{1/2}$. The backbone C and the AB side chains are modeled as flexible Gaussian chains within the mean-field approximation.[1] Herein, the canonical partition function of a melt of a bottlebrush polymer with ABC blocks can be written as[2]

$$\frac{F}{\alpha n k_b T} = \frac{1}{V}\int dr\left[\sum_{i<j} N\chi'_{ij}\phi_i(r)\phi_j(r) - \sum_j W_j(r)\phi_j(r) - P\left(1-\sum_j \phi_j(r)\right)\right] - \frac{1}{\alpha}\ln Q[W_i] \qquad \text{(S1)}$$

The interaction energy between dissimilar species A, B, and C is described by a Flory-like model through the Flory-Huggins parameter χ'_{ij}. We employ a dimensionless monomer volume fraction $\phi_j = \rho_j/\rho_0$ in the free energy expression ($\rho_0 = nN_t/V$). $Q[W_i]$ is the partition function of a non-

interacting polymer in external fields $W_i(r)$ that can be expressed in terms of a restricted chain partition function $q(r,s)$ as will be discussed below. The polymer is assumed to be incompressible, a constraint enforced through a pressure field $P(r)$. k_bT is the thermal energy. The architecture of the bottlebrush molecule is constructed using propagators $q_j(r, s, k)$ and $q_j^+(r, s, k)$ where s is a variable parameterizing the contour of chain for segment number k. The polymer probability distributions q_i and q_i^+ satisfy the modified diffusion equation

$$\frac{\partial}{\partial s} q = R_g^2 \nabla^2 q - W_i q \tag{S2}$$

Hence, the applied field W_i matches the block type of contour variable s when solving eq. (2). The key step in constructing the polymer structure is identifying the initial conditions for every propagator. In this regard, $q_A(r,0,k) = q_B(r,0,k) = 1$; $q_C(r,0,1) = q^+_C(r,0,m+1) = 1$; $q_C(r,0,k+1) = q_A(r,N_A,k)q_B(r,N_B,k)q_C(r,N_C,k)$; $q^+_A(r,0,k) = q_B(r,N_B,k)\ q_C(r,N_C,k)q^+_C(r,N_C,m+1-k)$; $q_B^+(r,0,k) = q_A(r,N_A,k)q_C(r,N_C,k)q^+_C(r,N_C,m+1-k)$; $q^+_C(r,0,k) = q_A(r,N_A,k)q_B(r,N_B,k)\ q^+_C(r,N_C,k-1)$ where $k \in [1,m]$. The modified diffusion equation is solved using the pseudospectral method with operator splitting scheme.[3] Accordingly, the single chain partition function can be written as $Q = 1/V \int dr\ q_C(r, N_C, m+1)$. Minimization of the free energy F with respect to the fields, density, and pressure leads to the following set of equations that have to be solved self-consistently.[3]

$$\begin{aligned}
\phi_A &= \frac{1}{QN_t} \sum_{k=1}^{m} \int_0^{N_A} ds q_A(r,s,k) q_A^+(r, N_A - s, k) \\
\phi_B &= \frac{1}{QN_t} \sum_{k=1}^{m} \int_0^{N_B} ds q_B(r,s,k) q_B^+(r, N_B - s, k) \\
\phi_C &= \frac{1}{QN_t} \sum_{k=1}^{m+1} \int_0^{N_C} ds q_C(r,s,k) q_C^+(r, N_C - s, k) \\
W_A(r) &= \chi'_{AB} N\phi_B(r) + \chi'_{AC} N\phi_C(r) + P(r) \\
W_B(r) &= \chi'_{AB} N\phi_A(r) + \chi'_{BC} N\phi_C(r) + P(r) \\
W_C(r) &= \chi'_{AC} N\phi_A(r) + \chi'_{BC} N\phi_B(r) + P(r) \\
\phi_A(r) &+ \phi_B(r) + \phi_C(r) = 1
\end{aligned} \tag{S3}$$

The numerical solution of the SCFT equations to study phase separation of the bottlebrush polymer can be initialized through random fields W_i's or seeded with initial structures, which are subsequently used to solve the modified diffusion eq. (2). The calculated propagators are employed

to estimate Q and accordingly the density distributions. The fields W_i's and P are updated using a numerical relaxation scheme.[4] The effect of confinement on the polymer domains is depicted through a masking method. External fields of $W_i = 10$ are imposed as masks at the location of the walls at a thickness of 6 pixels each to create a polymer free region.

The analysis focuses on densely packed bottlebrush polymers with a short linker between grafted chains. Hence, we set $N_C/N = 0.02$ with a large value of $m = 29$.[5] For comparison, calculations are also conducted for a bottlebrush polymer with m =1 which closely resembles a diblock polymer with a single AB chain and two very short branches of C. Block C is assumed to be neutral towards either of the two remaining blocks ($\chi'_{AC} = \chi'_{BC} = 0$), and only contributes to the AB interface with an entropic constraint on the AB chain spacing. The distribution of C in the polymer morphology is a response to the AB segregation governed by the incompressibility constraint of SCFT. For equal proportions of AB ($N_A = N_B$), the polymer forms striped structures with flat interfaces independent of χ'_{AB} and m, forcing C to be localized at the AB interface. Furthermore, it was shown that effective degree of segregation between the AB blocks had a strong dependence on m where grafting more chains on the polymer backbone caused the polymer to phase separate at a lower χ.[5] In order to isolate the structural effects on the polymer for different values of m, we use a rescaled value of χ between the AB blocks where $\chi'_{AB} = \alpha\chi / m$.[6] We assume that the polymer exhibits an intermediate degree of segregation of $\chi N = 25$.

Fitting free energy plots

Bita et al. derived a model describing the change of ΔF as polymer domains are strained away from their equilibrium periodicity L_0. The expression takes into account both the conformational entropy of a polymer chain and the interfacial energy between domains. The expression reads

$$\frac{\Delta F}{k_b T} = x(N,b)D^2 + y(N,\chi,b)/D + z$$

$$x = \frac{1}{8Nb^2}; y = 2Nb\sqrt{\frac{\chi}{6}} + 2b\sqrt{N}; z = -3/2 \qquad \text{(S4)}$$

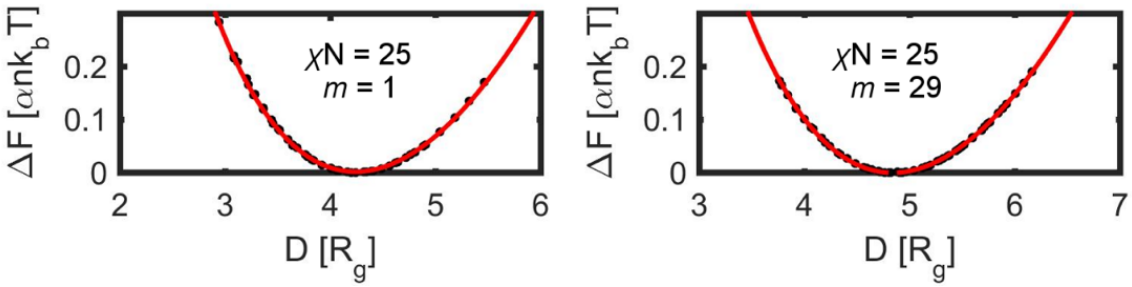

Figure S10. Master free energy showing the effect of trench spacing in real units [R_g] on polymer strain energy.

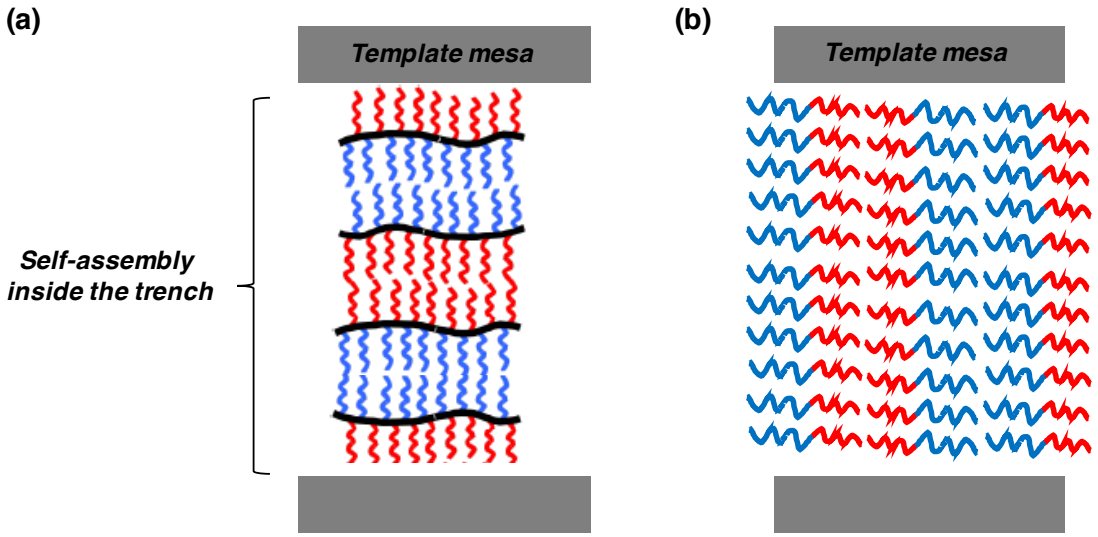

Figure S11. Schematic representation of (a) extended backbone of BBCP being parallel to the wall (parallel domain orientation) and (b) BCP sidechains being parallel to the wall (perpendicular domain orientation).

References

(1) Helfand, E. *J. Chem. Phys.* **1975**, *62* (3), 999–1005.

(2) Lee, W. B.; Elliott, R.; Mezzenga, R.; Fredrickson, G. H. *Macromolecules* **2009**, *42* (3), 849–859.

(3) Rasmussen, K.; Kalosakas, G. *J. Polym. Sci. Part B Polym. Phys.* **2002**, *40* (16), 1777–1783.

(4) Sides, S. W.; Fredrickson, G. H. *Polymer (Guildf).* **2003**, *44* (19), 5859–5866.

(5) Kawamoto, K.; Zhong, M.; Gadelrab, K. R.; Cheng, L. C.; Ross, C. A.; Alexander-Katz, A.; Johnson, J. A. *J. Am. Chem. Soc.* **2016**, *138* (36), 11501–11504.

(6) Zhang, L.; Lin, J.; Lin, S. *J. Phys. Chem. B* **2008**, *112* (32), 9720–9728.